Spin and valley half metal induced by staggered potential and magnetization in silicene*

Wang Sa-Ke(汪萨克), Tian Hong-Yu(田宏玉), Yang Yong-Hong(杨永宏), and Wang Jun(汪 军)†

Department of Physics, Southeast University, Nanjing 210096, *China*

(Received 8 May 2013; revised manuscript received 5 August 2013; published 3 December 2013)

We investigate the electron transport in silicene with both staggered electric potential and magnetization; the latter comes from the magnetic proximity effect by depositing silicene on a magnetic insulator. It is shown that the silicene could be a spin and valley half metal under appropriate parameters when the spin–orbit interaction is considered; further, the filtered spin and valley could be controlled by modulating the staggered potential or magnetization. It is also found that in the spin-valve structure of silicene, not only can the antiparallel magnetization configuration significantly reduce the valve-structure conductance, but the reversing staggered electric potential can cause a high-performance magnetoresistance due to the spin and valley blocking effects. Our findings show that the silicene might be an ideal basis for the spin and valley filter analyzer devices.

Keywords: silicene, spin–orbit interaction, spin and valley half metal, spin and valley blocking effect

PACS: 72.25.Dc, 72.80.Vp, 73.20.At **DOI:** 10.1088/1674-1056/23/1/017203

1. Introduction

Since the successful isolation of a single layer of carbon atoms from graphite, graphene has sparked a flurry of research activity.[1–5] The honeycomb lattice structure of graphene leads to a linear energy dispersion of the low-energy particles, which is described by the massless Dirac equation. The most fascinating electronic properties[4,5] of graphene arise from the Dirac-like excitations around the K and $K' = -K$ valleys of the Brillouin zone. However, the zero energy gap in graphene and the Klein tunneling of chiral particles limit the performance of graphene-based conventional electronic devices like diodes and transistors. Also, since the spin–orbit coupling (SOC) in graphene is quite small and therefore neglected, interesting effects, such as the induced spin–valley coupling discussed in this work, are not evident. The predicted quantum spin Hall insulator in a graphene system by Kane and Mele[6] is also difficult to observe in experiment. Due to the application limitations of graphene, research attention began to turn to other 2D crystals which have graphene-like features but stronger spin–orbit coupling, such as silicene,[7–15] MoS_2[16–19] and germanene.[9] Currently, MoS_2 has been the subject of several experimental investigations and a single layer of MoS_2 can be exploited with different methods. Silicene, a single layer of silicon atoms with a honeycomb lattice structure, begins to emerge in laboratories,[20,21] e.g., Vogt *et al.*[22,23] synthesized successfully the single-layer silicene and confirmed the predicted electronic structures and properties by measurements of scanning tunneling microscopy and angular-resolved photoemission spectroscopy. In comparison with other 2D graphene-like materials, the silicene seems more attractive since the silicon-based semiconductor electronics is very mature and a large silicon manufacturing industry is in place.

Silicene has two salient properties,[9] one is the bucked lattice structure owing to the large ionic radius of silicon, that is, one sublattice (say, an A-type silicon atom layer) is shifted upwards out of the 2D plane relative to the other one (a B-type silicon atom layer); the other is a relatively large SOC strength leading to a sizeable energy gap of about 1.55 meV, which provides a mass to the Dirac electrons so that one can control experimentally the mass by applying an electric field E_z. Theoretical works[11–15] showed very abundant phases of the silicene system within external electric, magnetic and optical fields. For example, with an increase of E_z, silicene undergoes a topological phase transition[11] from a quantum spin Hall (QSH) state to a band insulator (BI), where the QSH state is characterized by a full insulating gap in the bulk and helical gapless edges. When a uniform magnetization from either a magnetic field or the magnetic proximity effect is considered in silicene, much more phases were identified in the parameter space by Ezawa,[13] such as the quantum anomalous Hall state (QAH), the valley polarized metal state (VPM) and the marginal and spin VPM.

When the magnetization in silicene is assumed from the magnetic proximity effect by depositing the silicene on a magnetic insulator, such as EuO or $Y_3Fe_5O_{12}$,[24,25] the magnetization magnitude in different sublattices (A and B silicon atom layers) could be different due to the bucked lattice structure. This is because the proximity effect[24] strength is related to

*Project supported by the National Natural Science Foundation of China (Grant Nos. 11074032, 11074233, and 11274079) and the Natural Science Foundation of Jiangsu Province, China (Grant No. BK20131284).

†Corresponding author. E-mail: jwang@seu.edu.cn

© 2014 Chinese Physical Society and IOP Publishing Ltd

the electron hopping between two atoms, which decreases significantly with the spatial distance; therefore, a staggered magnetization could be present in the silicene and may produce a different effect on the electron transport from the uniform magnetization, which has been studied in Ref. [13]. In this work, we investigate the electron transport properties of silicene by considering both staggered sublattice potential from the E_z field and magnetization from the magnetic proximity effect. We show that there exist both spin and valley half metal states in appropriate parameter space: one spin (valley) band is metallic whereas the opposite spin (valley) band exhibits an energy gap at the Fermi surface. The numerical calculations in a lattice model demonstrate that the silicene could be an ideal spin and valley filter and analyzer; further, the active spin and valley state could be controlled by either electric field E_z or magnetization M. A silicene spin-valve structure is also studied and the conductance can be significantly modulated by both reversing the E_z and M directions.

2. Model and phase diagram

Similar to the graphene lattice structure, silicene consists of a honeycomb lattice of silicon atoms with two sublattices made of A sites and B sites. However, it has a bucked structure in which the two sublattice planes are separated by a distance l. Within an external electric field E_z, a staggered sublattice potential between silicon atoms at A sites and B sites is generated; it can induce a controllable energy gap of the low-energy particle at both K and K' valleys. A relatively large energy gap about 1.55 meV from the SOC has been found in silicene by the density functional theory and can be enhanced further by a strain.[9] When a 2D silicene is deposited on a magnetic insulator, as schematically shown in Fig. 1(a), the magnetizations at both A and B silicon sites are induced but with different magnitudes M_A and M_B. Based on the tight-binding model of the π orbits of the silicon atoms, the Hamiltonian of the system is given by

$$H = -t\sum_{\langle ij\rangle\alpha} C^{\dagger}_{i\alpha}C_{j\alpha} + \frac{i\lambda}{3\sqrt{3}}\sum_{\langle\langle ij\rangle\rangle\alpha\beta} v_{ij}C^{\dagger}_{i\alpha}\sigma^{z}C_{j\beta} - \sum_{i\alpha}\mu_i\Delta C^{\dagger}_{i\alpha}C_{i\alpha} + \sum_{\alpha\beta}C^{\dagger}_{i\alpha}M_i\sigma^{z}C_{i\beta}, \quad (1)$$

where $C^{\dagger}_{i\alpha(\beta)}$ ($C_{i\alpha(\beta)}$) is the electron creation (annihilation) operator at site i with spin polarization α (β) and $\langle ij\rangle$ ($\langle\langle ij\rangle\rangle$) denotes the summation over the nearest (next-nearest) neighbor lattice sites. The first term describes the π-orbit hopping among the nearest neighbor sites with the hopping integral t. The second term is the effective spin–orbital coupling term with strength λ; σ^i ($i = x, y, z$) is the Pauli matrix, $v_{ij} = 1$ if the next-nearest-neighboring hopping is anticlockwise and $v_{ij} = -1$ if it is clockwise with respect to the positive z axis. The 3rd term represents the staggered lattice potential $\Delta = E_z l$ induced by the electric field E_z, where $\mu = +1$ (-1) for the A (B) site. The last term is the magnetization M_i at each site from the magnetic proximity effect and the magnetization direction is assumed along the z axis. The magnetization M_A at A sites may be different from M_B at B sites. It is noted here that the Rashba spin–orbital interaction is neglected since its strength is an order of magnitude smaller than the other energy scales, such as the intrinsic SOC strength λ.

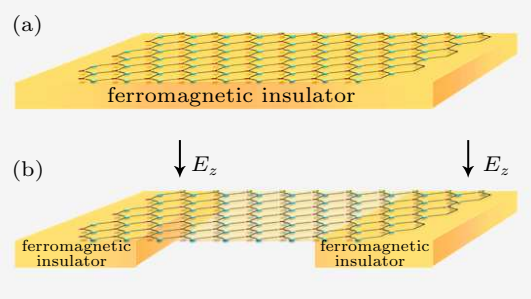


Fig. 1. (color online) Schematic diagrams of (a) a two-dimensional silicene deposited on a ferromagnetic insulator and (b) a spin-valve structure of silicene. The staggered electric potential is induced in silicene by the external electric field E_z as well as the staggered magnetization from the magnetic proximity effect.

By projecting Eq. (1) onto the momentum space and then expanding it at K and K' valleys, one can obtain the following low-energy effective Dirac-type Hamiltonian[13]

$$H_\eta = \hbar v_F(\eta k_x\tau_x + k_y\tau_y) + \lambda\eta\tau_z\sigma_z - \Delta\tau_z + M\sigma_z + m\tau_z\sigma_z, \quad (2)$$

where η is the valley label for the two opposite valleys K and K' and $k_{x(y)}$ is the $x(y)$-component momentum of particles. The matrices τ_i and σ_i ($i = x, y, z$) are the Pauli matrices; the former acts on the pseudospin space associated with the A and B sublattices while the latter is for real spins. Here, $v_F = \sqrt{3}at/2$ is the Fermi velocity and a is the lattice constant; $M = (M_A + M_B)/2$ and $m = (M_A - M_B)/2$ denote the average magnetization and the relative magnetization difference between the two sublattice atoms, respectively. When $m = 0$ and $M \neq 0$, a uniform magnetization exists in silicene and this case corresponds also to an external magnetic field applied on the system. The $m \neq 0$ case denotes a staggered magnetization in silicene and the magnetic proximity effect accounts for it. When $M = 0$ and $m \neq 0$, the silicene in the antiferromagnetic order can exhibit abundant phases, such as the single Dirac cone phase, that is, one valley gap exists whereas the opposite valley displays a semi-metallic state.[14]

The spin and valley dependent eigenvalues can be evaluated from the Hamiltonian above

$$E_{\eta\sigma} = M\sigma \pm \sqrt{\hbar^2 v_F^2(k_x^2 + k_y^2) + (\lambda\eta\sigma + \Delta + m\sigma)^2}, \quad (3)$$

where $\eta = \pm 1$ and $\sigma = \pm 1$ are respectively the valley and spin indices. It is seen that in the absence of magnetization $M = m = 0$, there is an energy gap at the Fermi surface opened by the SOC and the staggered potential Δ, so the system is a bulk insulator. Actually, due to the SOC, the system has the

Z_2 topological order and the energy gap closes at the edges of silicene when $\Delta < \lambda$, which is in the topological insulator or QSH insulator state.[13] At critical points $\lambda = \pm\Delta$, one spin (valley) energy gap is closed to give a Dirac point while the opposite spin (valley) band is still gapped; however, at Fermi surface $E_F = 0$, the density of states is still zero. When the staggered magnetization is introduced $m \neq 0$, the energy gap at one spin (valley) band may be present while the other spin (valley) band may possess nonzero density states at the Fermi energy, which is referred to as a spin (valley) half metal.

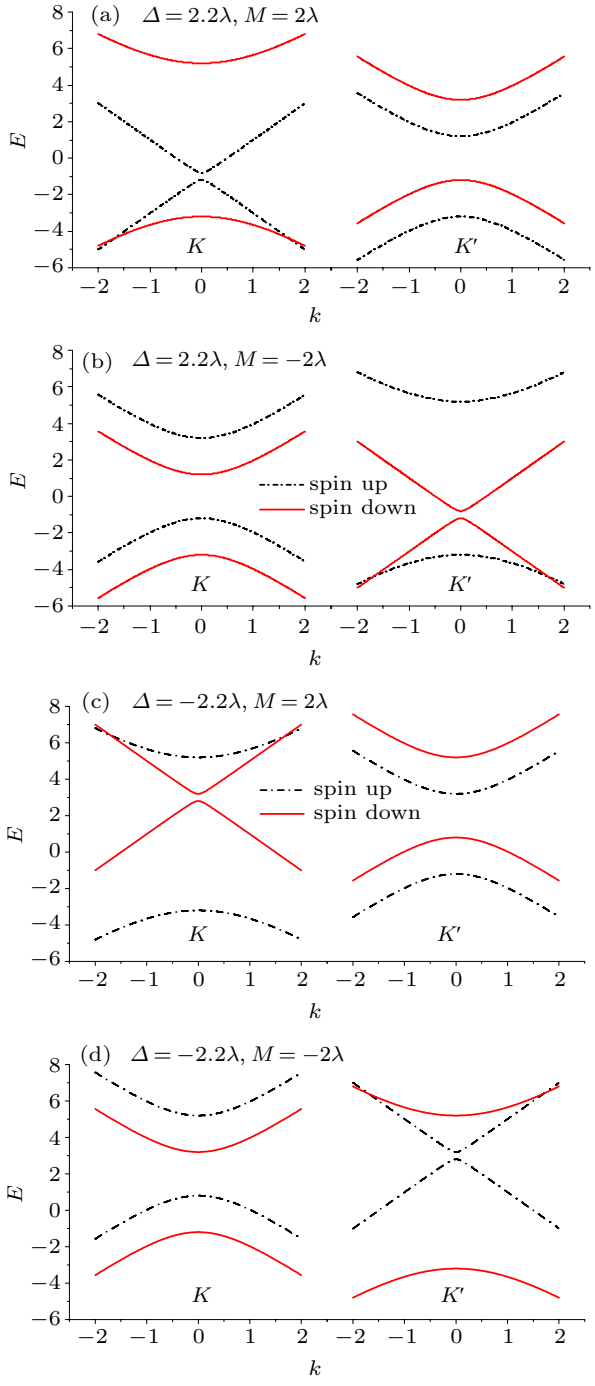


Fig. 2. (color online) Energy dispersions of a bulk silicene system with both the staggered electric field and magnetization for ((a)–(d)) different parameters Δ and M. Parameters are $\hbar V_F = 1$ and $M = m$.

In Fig. 2, we plot the particle E–k dispersion of silicene for different parameters Δ and M. Here, an extreme case of the magnetization $M = m$ is considered, in which the magnetization at B silicon sites are neglected $M_B = 0$. It is shown in Fig. 2(a) that an energy gap is present at the K' valley, whereas at the K valley, the Fermi surface $E_F = 0$ transverses the spin-up band, so the system is not only a spin half metal but a valley half metal. However, which spin (valley) band is open or closed at the Fermi surface crucially depends on Δ and M. When the magnetization M is reversed, as shown in Fig. 2(b), the active spin state at E_F is reversed and more importantly, the valley state is also reverse, i.e., the K valley band is now gapped at E_F whereas the K' valley is metallic. This is due to the effective SOC term $\lambda\eta\sigma$. When the electric potential Δ from electric field E_z is reversed in Fig. 2(c), the spin state at E_F is also reversed in comparison with that in Fig. 2(a) but the K valley is still conductive; nevertheless, the particle type transfers from the electron-like type to the hole-like one. In Fig. 2(d), when both Δ and M are reversed, the filtered spin state is unchanged but the active valley state and particle type are changed; therefore, the results in Fig. 2(d) are actually the superposition of those in Figs. 2(b) and 2(c).

In Fig. 3(a), we plot the phase diagram of silicene in the Δ and M space from Eq. (3). The QSH insulator survives in weak staggered potential Δ and magnetization M, $|D| < \lambda$ and $|M| < \lambda$, where E_F lies in the bulk energy gap and the Chern number and the spin-Chern number are given by $C = 0$ and $C_s = 1$, respectively. Outside this QSH region, the system exhibits a BI state, a spin and valley half-metal state, or a pure metallic state. In the four half-metal regions, the metallic states have different spin and valley indices, as marked in Fig. 3(a). The pure metallic state at the strong magnetization regions has nonzero density of states for both the two spin and two valley states at E_F; actually, this pure metal is termed as the valley polarized metal (VPM).[13] There also exist pure valley half-metal states (KH and K'H) in which both the two spin channels are open. Certainly, the spin and valley half-metal states appear due to the staggered magnetization $2m = M_A - M_B \neq 0$. Therefore, when m decreases, the half-metal regions are seriously suppressed as shown in Fig. 3(b) and mainly survive at both strong magnetization M and electric potential Δ. When $m = 0$, the half-metal state entirely evolves to the VPM state, as studied in Ref. [13]. It is noted that the half-metal states still have spin-polarized edge states and dissipationless currents flowing at the edges of silicene, which can exhibit the anomalous Hall effect, the spin and valley-polarized Hall effect. However, the Hall conductivity is not quantized since one spin or valley band is metallic.

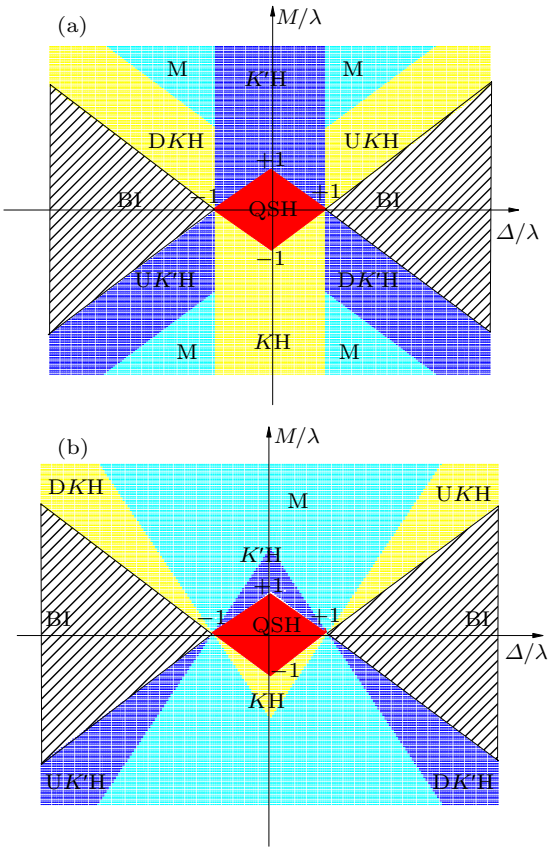


Fig. 3. (color online) Phase diagrams in the Δ–M plane with (a) $M_B = 0$ and (b) $M_B = M_A/2$. The different phases are the quantum spin Hall phase (QSH), the pure metallic phase (M), the spin-down (up) and K (K') valley half-metal phase (D(U)K (K')H), the K (K') valley half-metal phase (K (K')H) and the band insulator phase (BI).

3. Conductance and magnetoresistance

In this section, we calculate the conductances of the silicene nanoribbon devices according to the tight-binding Hamiltonian (Eq. (1)). Based on the nonequilibrium Green's function method, the conductance is given by[26,27]

$$G = \frac{e^2}{h}\mathrm{Tr}[\Gamma_L G^r \Gamma_R G^a], \tag{4}$$

where $\Gamma_{L(R)} = i(\Sigma_{L(R)} - \Sigma^{\dagger}_{L(R)})$ is the line width function with $\Sigma_{L(R)}$ the self-energy function of the left and right implicit ribbon leads, which is absent of any disorder or interaction influencing the particle energy. As a matter of fact, $\Gamma_{L(R)}$ also denotes the escaping rate of electrons and is proportional to the particle velocity. The $\Sigma_{L(R)}$ can be obtained from $\Sigma_{L(R)} = H_{s,L(R)} g_{L(R)} H^{\dagger}_{s,L(R)}$, where $H_{s,L(R)}$ is the coupling between the scattering region and the left (right) lead and $g_{L(R)}$ is the surface Green's function of the two ideal semi-infinite leads. The retarded Green's function $G^r = (G^a)^{\dagger} = [EI - H - \Sigma_L - \Sigma_R]^{-1}$ is calculated by a recursive method, where H is the Hamiltonian matrix in Eq. (1) and I is a unit matrix.

We first focus on the conductance of a uniform silicene nanoribbon with zigzag edges. In the calculations, the hopping energy t is set as the energy unit, $t = 1$, the SOC strength is taken as $\lambda = 0.03t$ and the temperature is taken as $T = 0$ K. In Fig. 4, the spin-resolved conductances are presented as a function of the Fermi energy E_F. It is shown that in all 4 panels, the system exhibits a spin half-metal behavior, i.e., at $E_F = 0$, one spin-species conductance is zero and the opposite spin-species current is allowed. In Fig. 4(a), as $\Delta > 0$, $M_A > 0$, the spin-up channel at $E_F = 0$ is open and the spin-down one is closed. Comparatively, when the electric field M is reversed, the blocked spin channel is also reversed as well as the prohibited energy range, as shown in Fig. 4(b). This is consistent with the band structures in Fig. 2. When the magnetization M is kept unchanged and Δ is reversed $\Delta < 0$ in Fig. 4(c), the active spin channel is opposite in comparison with that in Fig. 4(a), which also corresponds to the electronic band structure in Fig. 2. In Fig. 4, we do not show the valley-dependent conductances since they cannot be distinguished exactly due to the existence of edge states connecting the two valleys. The nonzero platforms of the single quantum conductance ($G = e^2/h$) come from the edge states.

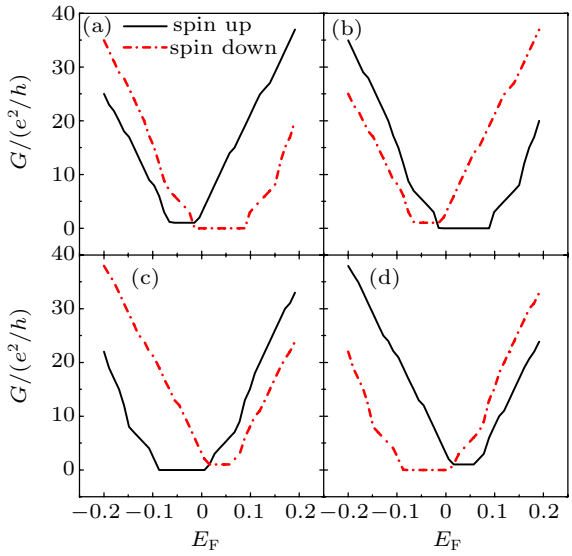


Fig. 4. (color online) Conductance of a uniform silicene zigzag nanoribbon. The zigzag chain number of the ribbon is $N = 256$ and $M_B = 0$, other parameters are $\Delta = 3\lambda$ and $M_A = 3.5\lambda$ in panel (a), $\Delta = 3\lambda$ and $M_A = -3.5\lambda$ in panel (b), $\Delta = -3\lambda$ and $M_A = 3.5\lambda$ in panel (c) and $\Delta = -3\lambda$ and $M_A = -3.5\lambda$ in panel (d).

Since the reversing electric field E_z can make the active spin channel reversed, it is possible to obtain a high-performance magnetoresistance by controlling E_z in a spin-valve structure. A schematic device is shown in Fig. 1(b), where the left and right silicene leads could have different magnetizations M and electric fields Δ, while the middle region is absent of any Δ and M and the magnetic insulator is not an electrode but only magnetizes the electrons in silicene.

In Fig. 5, the conductances of the spin-valve structure within the parallel and antiparallel structures are shown. When the left and right leads have the same Δ and M in the parallel configuration, the conductance G is comparatively large, as is seen from the solid line in Fig. 5, while in the electric-field

antiparallel structure by reversing E_z in one of the leads, the electric current of the system could be perfectly blocked and the conductance is zero in some energy regions, as indicated by the dashed line in Fig. 5. The usual antiparallel configuration by reversing M could also lead to a perfect magnetoresistance effect, as seen from the dash-dotted line. Different from the usual spin valve structure where the antiparallel magnetization is vital for blocking the current, the reversing electric field E_z in the silicene ribbon can exert the same effect. The reason has been mentioned above: the silicene could be an ideal spin and valley half metal, which depends crucially on Δ and M in some energy regions, where only one spin-species channel is active and the opposite one is closed.

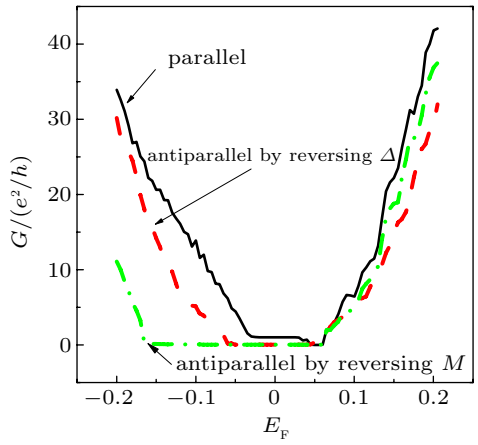


Fig. 5. (color online) Conductance of a spin-valve structure of silicene nanoribbon. The zigzag chain number of the ribbon is $N = 256$, the length of the middle between the left and the right is $L = 100a$, $M_B = 0$, $\Delta = 3.0\lambda$, $M_A = 3.5\lambda$ in the two leads and $M = m = 0$ and $\Delta = 0$ in the middle region of the structure. Different lines correspond to different spin-valve structures by reversing either M or Δ.

4. Summary and conclusion

In summary, we have investigated the electron transport in a single-layer silicene system by considering both the staggered electric potential and magnetization; the latter is assumed to come from the magnetic proximity effect and the different magnetizations in the A and B sites of silicene are due to the bucked lattice structure. It was shown that the silicene could be a perfect spin and/or valley half metal by controlling an external electric field and the magnetization. The relative magnetization m between the A and B silicon sites determines crucially the parameter region of the spin and valley half metal. The conductances of the silicene spin-valve structure were calculated and the efficient magnetoresistance effect was shown, not only by reversing the magnetization but also the electric field. Our results indicate that silicene could an ideal spin and valley filter and analyzer.

References

[1] Novoselov K S, Geim A K, Morozov S V, Jiang D, Katsnelson M I, Grigorieva I V, Dubonos S V and Firsov A A 2005 *Nature* **438** 197
[2] Zhang Y, Tan Y W, Stormer H L and Kim P 2005 *Nature* **438** 201
[3] Novoselov K S, McCann E, Morozov S V, Falko V I, Katsnelson M I, Zeitler U, Jiang D, Schedin F and Geim A K 2006 *Nat. Phys.* **2** 177
[4] Beenakker C W J 2008 *Rev. Mod. Phys.* **80** 1337
[5] Castro Neto A H, Guinea F, Peres N M R, Novoselov K S and Geim A K 2009 *Rev. Mod. Phys.* **81** 109
[6] Kane C L and Mele E J 2005 *Phys. Rev. Lett.* **95** 226801
[7] Vogt P, De Padova P, Quaresima C, Avila J, Frantzeskakis E, Asensio M C, Resta A, Ealet B and Lay G L 2012 *Phys. Rev. Lett.* **108** 155501
[8] Lin C L, Arafune R, Kawahara K, Tsukahara N, Minamitani E, Kim Y, Takagi N and Kawai M 2012 *Appl. Phys. Express* **5** 045802
[9] Liu C C, Feng W and Yao Y 2011 *Phys. Rev. Lett.* **107** 076802
[10] Liu C C, Jiang H and Yao Y 2011 *Phys. Rev. B* **84** 195430
[11] Ezawa M 2012 *New J. Phys.* **14** 033003
[12] Ezawa M 2012 *J. Phys. Soc. Jpn.* **81** 064705
[13] Ezawa M 2012 *Phys. Rev. Lett.* **109** 055502
[14] Ezawa M 2013 *Phys. Rev. Lett.* **110** 026603
[15] Stille L, Tabert C J and Nicol E J 2012 *Phys. Rev. B* **86** 195405
[16] Mak K F, Lee C, Hone J, Shan J and Heinz T F 2010 *Phys. Rev. Lett.* **105** 136805
[17] Mak K, He K, Shan J and Heinz T 2012 *Nat. Nanotechnol.* **7** 494
[18] Zeng H, Dai J, Yao W, Xiao D and Cui X 2012 *Nat. Nanotechnol.* **7** 490
[19] Sallen G, Bouet L, Marie X, Wang G, Zhu C R, Han W P, Lu Y, Tan P H, Amand T, Liu B L and Urbaszek B 2012 *Phys. Rev. B* **86** 081301
[20] Lalmi B, Oughaddou H, Enriquez H, Kara A, Vizzini S, Ealet B and Aufray B 2010 *Appl. Phys. Lett.* **97** 223109
[21] Padova P, Quaresima C, Ottaviani C, Sheverdyaeva P, Moras P, Carbone C, Topwal D, Olivieri B, Kara A, Oughaddou H, Aufray B and Lay G 2010 *Appl. Phys. Lett.* **96** 261905
[22] Vogt P, De Padova P, Quaresima C, Avila J, Frantzeskakis E, Asensio M C, Resta A, Ealet B and Le Lay G 2012 *Phys. Rev. Lett.* **108** 155501
[23] Fleurence A, Friedlein R, Ozaki T, Kawai H, Wang Y and Yamada-Takamura Y 2012 *Phys. Rev. Lett.* **108** 245501
[24] Haugen H, Huertas-Hernando D and Brataas A 2008 *Phys. Rev. B* **77** 115406
[25] Uchida K, Xiao J, Adachi H, Ohe J, Takahashi S, Ieda J, Ota T, Kajiwara T, Umezawa H, Kawai H, Bauer G E W, Maekawa S and Saitoh E 2010 *Nature Mater.* **9** 894
[26] Tian H Y, Yang Y H, Chan K S and Wang J 2012 *Phys. Rev. B* **86** 245413
[27] Wang J and Liu S 2012 *Phys. Rev. B* **85** 035402